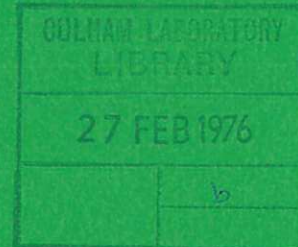


This document is intended for publication in a journal, and is made available on the understanding that extracts or references will not be published prior to publication of the original, without the consent of the authors.



UKAEA RESEARCH GROUP

Preprint

COMPUTATIONAL MODEL OF LASER INDUCED 'HOLE BURNING' IN A DENSE CARBON PLASMA

M M MICHAELIS
P T RUMSBY

CULHAM LABORATORY
Abingdon Oxfordshire

1975

CLM - P 439

This document is intended for publication in a journal or at a conference and is made available on the understanding that extracts or references will not be published prior to publication of the original, without the consent of the authors.

Enquiries about copyright and reproduction should be addressed to the Librarian, UKAEA, Culham Laboratory, Abingdon, Oxfordshire, England

COMPUTATIONAL MODEL OF LASER INDUCED
'HOLE BURNING' IN A DENSE CARBON PLASMA

by

M.M. MICHAELIS AND P.T. RUMSBY

Culham Laboratory, Abingdon, Oxon, OX14 3DB, UK
(Euratom/UKAEA Fusion Association)

ABSTRACT

A high density laser-produced carbon plasma is heated with the beam from a pulsed CO₂ laser. The resulting density depression is modelled by a 2D computer code.

(Submitted for publication in Physics Letters A)

October, 1975

In a previous letter [1], we presented experimental results demonstrating how a CO_2 laser was used to generate a density depression in a dense plasma created by a Nd laser focussed on a carbon target. It was mentioned that a 2 dimensional hydrodynamic code was being used to model the evolution of the density profiles, as diagnosed by holographic interferometry. In this letter we present results generated by this code.

A Eulerian code was written by the authors to compute density profiles in the sub-critical region only, where the maximum electron mean free path was $10 \mu\text{m}$ and the typical density gradient scale length was about 0.5 mm . The cell size was fixed at $100 \mu\text{m}$. Time steps were 1 ns . Initial values of electron temperature T_e , plasma radial and axial directed velocities v_R and v_z and ion density n_i were chosen compatible with the measured Nd laser carbon target experiments [1,2,3] and the theory of Puell [4].

To illustrate the way the program operates we take the CO_2 beam to have a flat topped radial power profile $P(r)$ and to converge as shown in Fig.1. Inverse bremsstrahlung absorption causes the electron temperature to rise in those cells directly in the path of the CO_2 laser beam (Fig.2a). The electron density increase due to ionization coupled with the increase in T_e leads to an increase in the electron pressure p_e . This increase in pressure drives the plasma radially outwards, the density change being greatest at the maxima of the pressure second differential (Fig.2a). (At points where the first differential is large, but the second zero, as much plasma enters the cell as leaves it.) Heat transport outwards is by electron thermal conduction and plasma thermal convection, the latter

being the dominant mechanism. Another important convection mechanism is that of directed plasma energy. Radiation reaching the critical surface is deposited there.

It should be noted that for a flat topped power profile, the density at the centre only begins to decay when the rarefaction front has reached the centre (Fig.2b). This process leaves a central hump at early times, which disappears once the rarefaction profile has steepened enough for a pressure balance to establish itself. This hump has been experimentally observed in CO_2 laser breakdown plasmas [5].

We now discuss the computational results arising when we model the experimental situation. We find that the plasma motion is dominated by the initial directed axial and radial velocities since the ion velocities acquired during heating are low due to the large inertia of the ions. In the central region electron temperatures up to $\sim 80\text{eV}$ are computed (initial $T_e = 5\text{eV}$) leading to an increase in the average ion charge state from 2 to 4. Three factors determine the shape of the depression formed, the axial power deposition, the beam profile and the initial radial velocities.

The depth of the depression formed is dominated by the axial power deposition. Fig.3a shows a typical series of power deposition profiles. It is seen that the point of maximum power deposition z_d , moves in towards the target with increasing time as outer regions of the plasma are heated. At early times the perturbation close to the target is small.

We characterize the radius of the depression at any axial position by r_p , the radius of peak density (Fig.2b). This is given by $r_p \approx r_b + v_{r_0} t + \Delta r$, where r_b is the beam radius, v_{r_0} is the initial

directed radial velocity and Δr is the change in beam radius caused by laser power deposition. During heating, the maximum density profile acquires the shape of an amphora-like open cavity. Very far from the target where both v_r and power deposition are small $r_p \sim r_b$. Closer to the target $r_p \gg r_b$ due to large values of v_r and high power deposition. Finally, very near the target, v_r is again small and $r_p \sim r_b + \Delta r$.

In Fig.3b, the interferogram presented in [1] has the beam profile (dashed line) and the computed locus of r_p (solid line) superimposed upon it. A reasonable match to maximum fringe differential is obtained. In Fig.3c, computed electron densities (dashed line) are superimposed on the already published measured densities.

Where perpendicular gradients in n_e and T_e exist we expect thermo-electric effects to give rise to magnetic field generation. For the experimentally measured axial density gradients and the computed radial temperature gradients we find that magnetic fields up to 1 kG should occur. These do not affect the plasma dynamics ($\beta \gg 1$).

In conclusion we note that for subcritical densities and moderate CO_2 laser powers ($\sim 10^{10} \text{ W cm}^{-2}$) the processes of inverse bremsstrahlung, hydrodynamic motion, ionization, electron thermal conduction and plasma thermal and directed energy convection give a good account of the CO_2 laser induced depression in a Nd laser-produced carbon plasma.

REFERENCES

- [1] P.T. Rumsby and M.M. Michaelis, Phys. Letts., 49A. (1974) 413.
- [2] P.T. Rumsby, J.W.M. Paul and M.M. Masoud, Plasma Phys., 16,
(1974) 969.
- [3] P.T. Rumsby and J.W.M. Paul, Plasma Phys., 16, (1974) 297
- [4] H. Puell, Z. Naturforsch, 25a, (1970) 1807.
- [5] M.C. Richardson, I E E E. J. Quant. Elec., QE-9, (1973) 1139.

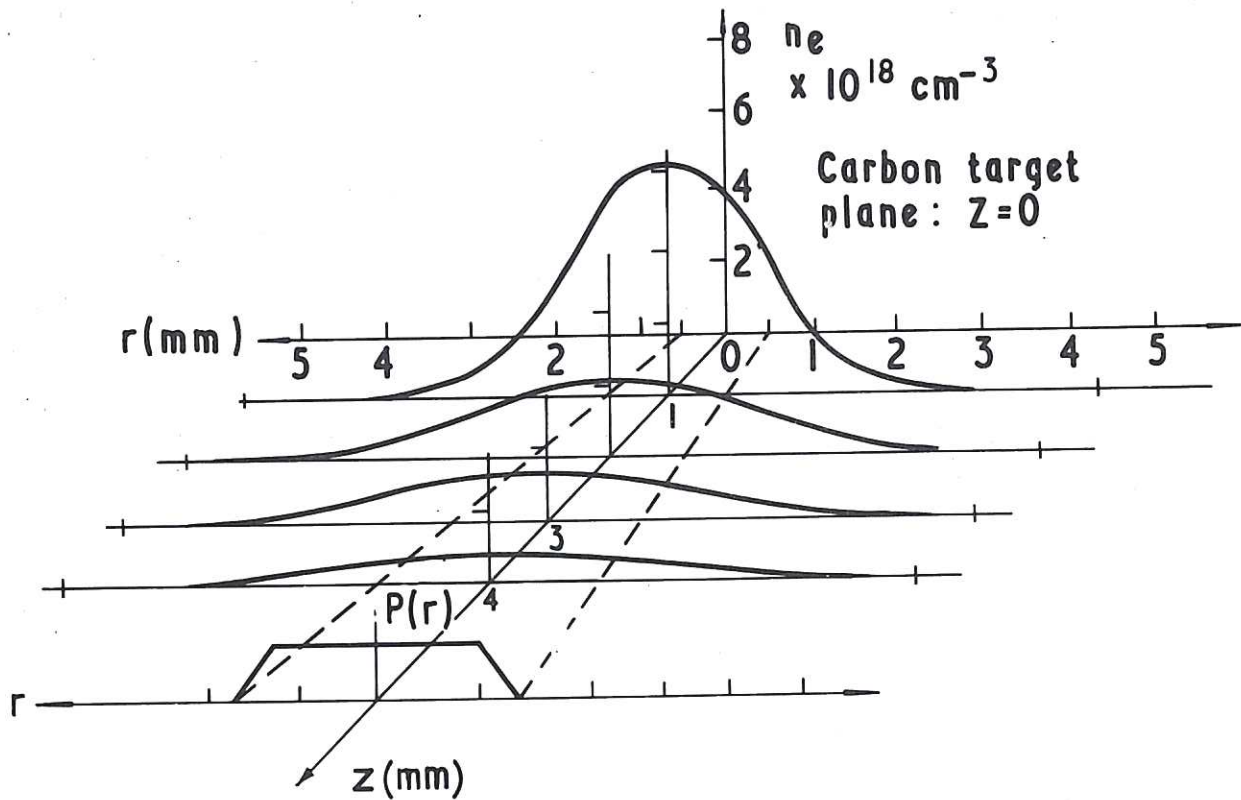


Fig.1 Initial values.

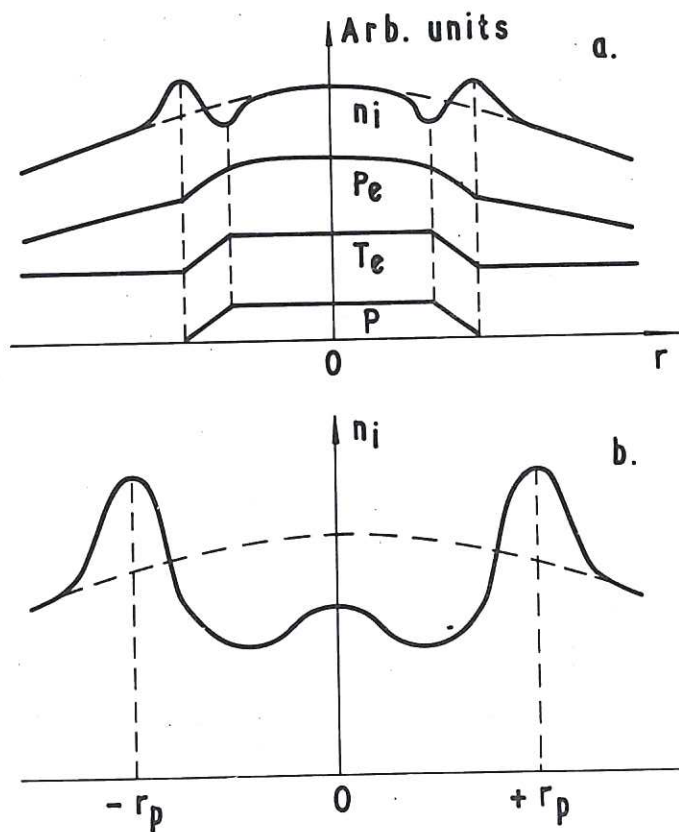


Fig.2 (a) Early and (b) late computation profiles (schematic).

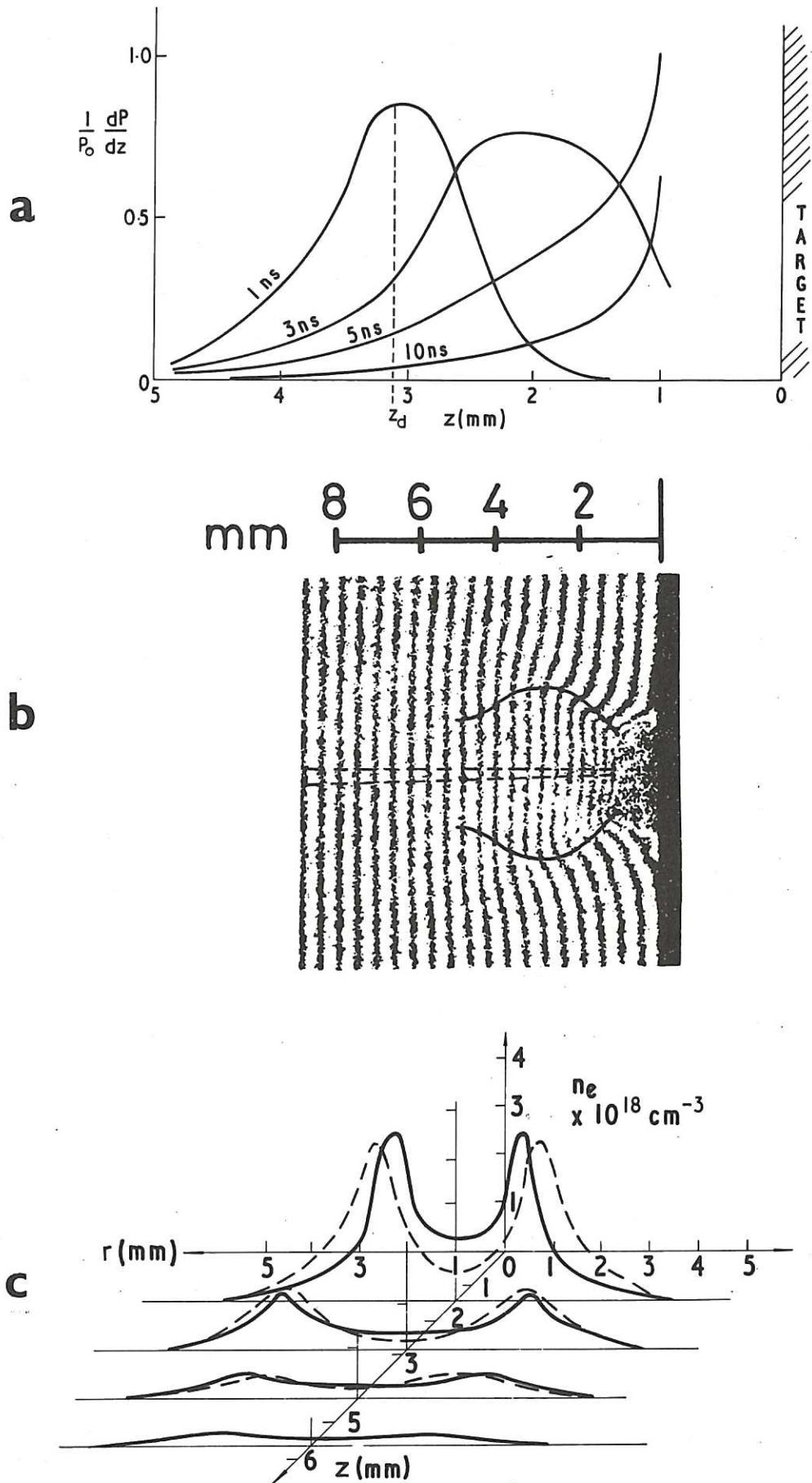


Fig.3 Computed and experimental parameters of reference [1]. (a) Normalised axial power deposition at the start of the CO₂ laser pulse. (b) Interferogram of density depression 22 ns after the peak of the CO₂ laser pulse. Solid line: computed locus of maximum density. Dashed line: laser beam diameter. (c) Density profiles corresponding to (b). Solid line: experimental. Dashed line: computational.

The first part of the document discusses the importance of maintaining accurate records of all transactions. It emphasizes that every entry, no matter how small, should be recorded to ensure the integrity of the financial data. This includes not only sales and purchases but also expenses and income. The document provides a detailed list of items that should be tracked, such as inventory levels, accounts payable, and accounts receivable. It also outlines the procedures for recording these transactions, including the use of double-entry bookkeeping to ensure that the books balance.

The second part of the document focuses on the analysis of the recorded data. It explains how to calculate key financial ratios and metrics, such as the gross profit margin, net profit margin, and return on investment. These calculations are essential for understanding the company's financial performance and identifying areas for improvement. The document also discusses the importance of comparing the company's performance against industry benchmarks and historical data to provide context for the results.

The final part of the document addresses the reporting requirements for the financial data. It details the format and content of the financial statements, including the balance sheet, income statement, and cash flow statement. It also discusses the importance of providing clear and concise explanations for the data presented in the reports, as well as the need to comply with relevant accounting standards and regulations.

